Stability analysis of functionally graded graphene platelets-reinforced nanocomposite shells

Farzad Ebrahimi [a, *], Amirhosein Effatmaneshfard [a], Hosein Ezzati [b], Salar Pashalou [b]

[a] *Department of Mechanical Engineering, Faculty of Engineering, Imam Khomeini International University, Qazvin, Iran*
[b] *School of Mechanical Engineering, College of Engineering, University of Tehran, Tehran, Iran*

Abstract

Investigating the stability of cylindrical shells made of composite materials is a valuable subject in mechanical engineering due to their plethora of usages across various industries. In the present investigation, the stability behavior of graphene platelets (GPLs) enhanced nanocomposite shells is methodically examined. The calculation of the composite material's properties is conducted by utilizing the modified rule of mixtures approach. Additionally, a first-order shear deformation theory is employed in conjunction with the principle of virtual work to establish the essential differential equations for the analysis. The solution to these equations is achieved by applying Galarkin's method, which is renowned for its accuracy and efficiency in resolving both static and dynamic problems. Verification of the formulated model is done by comparing the results with existing literature. Novel findings are presented showing the variation in buckling behavior of GPL-reinforced nanocomposite shells for assorted circumferential wave numbers. Moreover, the study delves into the impact of variations in GPLs' weight fraction, length and radius to thickness ratios, and the presence of an elastic medium on the critical buckling loads of these advanced composite shell structures.

Keywords: Buckling analysis; Graphene platelets nanocomposite; First-order shell theory

1. Introduction

Researchers' interest has recently been attracted by the extraordinary properties of nanocomposite materials reinforced with carbon derivatives. These materials, which are among the most often used reinforcements in nanocomposites and have remarkable chemical and physical characteristics, include carbon nanotubes (CNTs), graphene platelets (GPLs), carbon fibers, and graphene oxide powder (GOP). More precisely, because of their unique properties, GPLs have a wide range of possible applications across various industries. Numerous research has looked into the mechanical behavior of composite structures when carbon derivatives are added as nanoparticles. GPL-reinforced composites combine the exceptional qualities of GPLs with the benefits of a matrix material.

Herein, a summary of the considerable research on carbon derivative-reinforced nanocomposites is provided. Lee et al. [1] used nanoindentation in an atomic force microscope to measure the elastic properties and breaking strength of monolayer graphene membranes; these experiments demonstrated that graphene is a strong material, and that defect-free nanoscale materials can undergo substantial deformation beyond the linear regime. Rafiee et al. [2]

* Corresponding author. *E-mail address:* febrahimy@eng.ikiu.ac.ir

conducted a study on the bending of graphene/epoxy nanocomposite beams. By adding just 0.1% of graphene platelets to the epoxy, a significant increase in the beam's strength of up to 52% was observed. Formica et al. [3] accurately predicted the elastic moduli for various composites with aligned single-walled CNTs. Results show that CNT-reinforced rubber composites can achieve up to 500% increase in lowest natural frequency. Kolahchi et al. [4] explored the nonlinear dynamic stability analysis of temperature-dependent viscoelastic plates embedded with single-walled carbon nanotubes (SWCNTs). Furthermore, Nejati et al. [5] examined the thermal buckling behavior of cylindrical shells using the third-order shear deformation theory. The effects of CNT aspect ratio and waviness index on thermal buckling were analyzed to validate the formulation and explore the impact of parameters like volume fraction and distribution pattern of wavy CNTs. Barati et al. [6] investigated the post-buckling behavior of porous beams reinforced with graphene platelets, and their research demonstrated that nonlinear buckling and post-buckling behavior depends on the GPL distribution and porosity. Moreover, Yang et al. [7] explored the buckling and post buckling characteristics of nanocomposite beams with multiple layers. The nonlinear equations governing the behavior of the beam on an elastic foundation were derived based on the first-order shear deformation beam theory and subsequently their work showed that the addition of graphene platelets to nanocomposite beams on an elastic foundation improves their resistance to buckling and post-buckling.

In addition, Wang et al. [8] conducted a paper about the torsional buckling of cylindrical shells reinforced with GPLs. Using finite element method (FEM), they probed the impact of nanocomposite (NC)'s layer-count, GPL distribution, shell dimensions, GPL properties, the influence of cutout size, slenderness ratio, and orientation on NC's buckling behavior. Golabchi and his co-workers [9] presented an analysis of fluid velocity effects on the instability of pipes reinforced with silica nanoparticles (SiO2). Yang et al. [10] explored the buckling and vibration characteristics of porous nanocomposite plates reinforced with graphene platelets. They worked with multilayers and investigated the distribution patterns of reinforcement in a metal matrix. Also, the examination of the seismic response of underwater concrete pipes conveying fluid, which are coated with a nano-fiber reinforced polymer layer was carried out by Hajmohammad et al. [11]. Furthermore, Chen and Qiu [12] proposed a novel reliability assessment approach for fiber-reinforced composite laminates with correlated elastic parameters. They used non-statistical Grey mathematical theory and interval estimation methods to evaluate uncertainty and correlations. Hajmohammad and his team [13] Developed a novel numerical approach and applying a visco-refined zigzag theory for blast analysis of auxetic honeycomb plates featuring multiphase nanocomposite face sheets in a hygrothermal environment. Wang et al. [14] examined the buckling and post-buckling behaviors of dielectric composite beams reinforced with GPLs. It was shown that the behavior highly depends on frequency within a certain range, concentration, and the aspect ratio of GPLs. Results provided insights for developing GPL-based smart composites and structures. Zhou et al. [15] analyzed the buckling of cylindrical shells made of functionally graded porous graphene platelet reinforced composites under axial compressive load. Ebrahimi et al. [16] analyzed nanocomposite beams reinforced with GOP under a nonuniform magnetic field by using the Halpin-Tsai scheme and came to the conclusion that GOP distributions and beam models affect the stability. Qin et al. [17] Presented an unified solution for free vibration analysis of rotating functionally graded GPL-reinforced composite (FG-GPLRC) cylindrical shells and revealed that the variations of natural frequencies are highly dependent on boundary conditions. Also, Mahani et al. [18] researched the thermal buckling of functionally graded GPL-reinforced composite and investigated implementing a method called thermoelastic generalized differential quadrature (TE-GDQ). The outcome was influenced by multiple parameters including shell geometry, and length-to-thickness ratio at the critical temperature. In addition, Keshtegar et al. [19] studied the dynamic behavior of nanocomposite conical shells with magnetostrictive face sheets through the application of advanced sandwich panel theory. Yas and Rahimi [20] investigated the thermal buckling of porous nanocomposite beams with the help of the generalized differential quadrature method (GDQM) and also with the use of Gaussian random field (GRF) method for closed cell cellular solids they reached the mechanical properties. Keshtegar et al. [21] examined wave propagation and vibration in a beam with nanocomposite piezoelectric layers reinforced by different graphene nanoplatelet patterns.

More recently, Kolahchi et al. [22] focused on optimizing the dynamic buckling behavior of a laminated nanocomposite conical aircraft shell under various environmental conditions. Song et al. [23] investigated the nonlinear free vibration of edge-cracked composite beams reinforced with GPL. Furthermore, Zhang et al. [24] examined nanocomposite beams reinforced with single-layer GOPs. Abbaspour and Arvin [25] probed the buckling behavior of a three-layered rectangular nanocomposite microplate with graphene platelets. The buckling loads were determined using the Ritz method for different boundary conditions. Ebrahimi et al. [26] analyzed the buckling of GOP nanocomposite shells using Galerkin's method. Shahgholian et al. [27] studied the torsional buckling analysis of a cylindrical shell made of a composite material reinforced with GPLs using a mathematical model and computational simulations to calculate the critical buckling torque and the effect of porosity and mass density on the shell's performance. Shahgholian, et al. [28] studied the field of buckling in cylindrical shells under uniform lateral

pressure after exploring various porosity patterns. Furthermore, investigating the dynamic stability control of viscoelastic nanocomposite piezoelectric sandwich beams supported by Kerr foundation using the exponential piezoelasticity theory was carried out by Al-Furjan et al. [29]. Ansari et al .[30] investigated the post-buckling and free vibration of functionally graded graphene platelet (FG-GPL) reinforced nanocomposite plates with different shapes and porosities. Additionally, Al-Furjan et al. [31] analyzed the dynamic deflection and contact force histories of graphene platelets reinforced conical shells with integrated magnetostrictive layers under low-velocity impact conditions. Kolahchi et al. [32] proposed a numerical method to study the magneto-hygro-thermal dynamic stability of defective quadrilateral graphene sheets, incorporating higher order nonlocal strain gradient theory and various movable boundary conditions. Zheng et al. [33] spread graphene oxide powders throughout the metal foam plate in different patterns and found that vibration behavior depends on factors like the amount of graphene oxide, the support type, and temperature change. Sobhani et al. [34] explored the vibrational behavior of coupled hemispherical-conical shells made of composite materials reinforced with nanofillers. Ebrahimi et al. [35] conducted a study on wave propagation in 27-reinforced nanocomposite plates under thermal loading. Sobhani et al. [36] compared the effects of three nanofiller materials CNT, GNP, and GOP on the free vibration behavior of nanocomposite cylindrical shells. Alongside that, Guo and Arvin [37] worked on reducing the thermal buckling stiffness for certain patterns and also worked on the instability and post-instability response of a rotating nanocomposite beam. Zhaochao Li et al. [38] introduced an approach to rehabilitate pipelines made of functionally graded porous metal and graphene platelets. Ahmadi et al. [39] investigated the post-buckling behavior of an advanced porous nanocomposite plate reinforced with GOP. Xiang et al. [40] investigated the wave propagation in a curved nanocomposite beam reinforced with graphene oxide powder under different thermal loadings. In addition, an analytical method was utilized by Ebrahimi et al. [41] to determine the wave propagation of functionally graded nanocomposite plates reinforced with GPLs in presence of thermal loading. Finally, Bi et al. [42] focused on how thick rings behave after the bucking point and how their shape changes in post-buckling.

Although there has been considerable study into GPL reinforced nanocomposites and various related constructs, the literature still lacks an inquiry into the buckling characteristics within GPLR shell structures. As mentioned earlier, studying the durability and reliability of composite material cylindrical shells is an important area of research in the field of mechanical engineering. These structures are widely utilized in a variety of industries, making it crucial to understand how they perform under different conditions and loads. This study offers a comprehensive assessment of buckling behaviors in GPL-reinforced nanocomposite shells under an array of various parameters including circumferential wave number, GPL weigh fraction, length and radius to thickness ratios, and Winkler-Pasternak substrate coefficients. In this work, the critical buckling load determination of nanocomposite shells is addressed by synergizing the first-order shear deformation shell theory with the static form of the virtual work principle. Consideration is given to the cylindrical structure as it resides on a bi-parametric elastic medium that combines characteristics of linear and shear components. To address the computational aspects, the equations of motion are resolved using the renowned Galerkin's method, specifically tailored for systems with simply-supported (S-S) boundary conditions (BC).

2. Theory & Formulation

2.1. Material Homogenization

In this part, the Halpin-Tsai micromechanical model is utilized to achieve the mechanical properties of GPL-reinforced NC shell. Herein, subscripts: M and GPL represent matrix and GPL, respectively. Ensuing, the volume fraction of GPL fibers can be calculated as [43]:

$$V_{GPL}^* = \frac{W_{GPL}}{W_{GPL} + \left(\frac{\rho_{GPL}}{\rho_M}\right)(1 - W_{GPL})} \tag{1}$$

Where W and ρ stand for weight fraction and mass density, respectively. To calculate the effective Young's modulus of the resultant composite we can use the following formulation:

$$E_{eff} = 0.49E_l + 0.51E_t \tag{2}$$

E_l and E_t denote the longitudinal and transverse Young's moduli of the composite, respectively. these elastic parameters can be formulated as [43]:

$$E_l = \frac{1 + \xi_l \eta_l V_{GPL}}{1 - \eta_l V_{GPL}} \times E_M, \qquad E_t = \frac{1 + \xi_t \eta_t V_{GPL}}{1 - \eta_t V_{GPL}} \times E_M \tag{3}$$
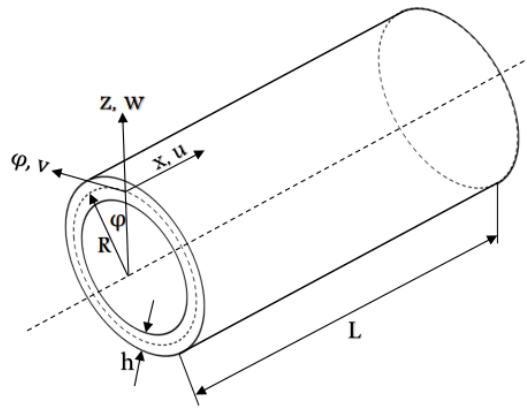
Where [44]:

$$\eta_l = \frac{\left(\frac{E_{GPL}}{E_M}\right) - 1}{\left(\frac{E_{GPL}}{E_M}\right) + \xi_l}, \qquad \eta_t = \frac{\left(\frac{E_{GPL}}{E_M}\right) - 1}{\left(\frac{E_{GPL}}{E_M}\right) + \xi_t} \tag{4}$$

In which, E_{GPL} and E_M account for GPLs and matrix Young's modulus. ξ_l and ξ_t represent the geometry factors and can be calculated by the following equation [44]:

$$\xi_l = \xi_t = \frac{2d_{GPL}}{h_{GPL}} \tag{5}$$

Where d_{GPL} and h_{GPL} are the parameters for the diameter and thickness of GPLs, respectively.

Figure 1. Geometry and coordinate system of a cylindrical shell

To calculate the effective Poisson's ratio, rule of mixture is utilized as:

$$v_{eff} = v_{GPL} V_{GPL} + v_M V_M \tag{6}$$

Where V_{GPL} and V_M are related to volume fractions of GPLs and matrix, in that order. According to the following equation, the matrix and the volume fractions of GPLs are related to each other as:

$$V_{GPL} + V_M = 1 \tag{7}$$

2.2. First-order shear deformable shell theory

In this section, the kinematic relations of a nanocomposite shell will be determined by using the first-order shear deformation theory for shells. However, in studies that are about thin-walled, shell-like elements the classical theory

of shells is more efficient in computational costs and still has accurate results [45].

The illustration in Figure 1 depicts the structure's geometry and coordinate system. Subsequently, the displacement fields of a shell, according to the first-order shear deformable shell theory can be articulated as:

$$u_x(x,\phi,z,t) = u(x,\phi,t) + z\theta_x(x,\phi,t)$$
$$u_\phi(x,\phi,z,t) = v(x,\phi,t) + z\theta_\phi(x,\phi,t)$$
$$u_z(x,\phi,z,t) = w(x,\phi,t)$$
(8)

In which, the displacements u, v, and w show how the structure moves in different directions related to axial, circumferential, and lateral displacements, respectively. Also, θ_x and θ_ϕ represent rotation components about axial and circumferential directions, respectively. Now, describing the nonzero strains experienced by the shell-type element can be determined by the following equations:

$$\varepsilon_{xx} = \frac{\partial u}{\partial x} + z\frac{\partial \theta_x}{\partial x}, \varepsilon_{\phi\phi} = \frac{1}{R}\left(\frac{\partial v}{\partial \phi} + z\frac{\partial \theta_\phi}{\partial \phi} + w\right)$$
$$\varepsilon_{x\phi} = \frac{1}{R}\frac{\partial u}{\partial \phi} + \frac{\partial v}{\partial x} + \frac{z}{R}\frac{\partial \theta_x}{\partial \phi} + z\frac{\partial \theta \phi}{\partial x}$$
$$\varepsilon_{xz} = \theta_x + \frac{\partial w}{\partial x}, \varepsilon_{\phi z} = \theta_\phi + \frac{1}{R}\frac{\partial w}{\partial \phi} - \frac{v}{R}$$
(9)

Where R is the radius of the cylinder introduced in Figure 1.

2.3. Derivation of motion equations

Using an extension of the principle of virtual work to analyze cylindrical shells in a nanocomposite material leads to deriving the Euler-Lagrange equations. This principle can be implemented in the following form:

$$\int_0^t \delta(U - V)dt = 0$$
(10)

In which strain energy, U, and the work done by external loads, V, for linear elastic materials are denoted. The variation of strain energy for a linear elastic solid can be formulated as:

$$\delta U = \int_{-\frac{h}{2}}^{\frac{h}{2}} \int_0^{2\pi} \int_0^L \sigma_{ij}\, \delta\, \varepsilon_{ij}\, R\, dx\, d\phi\, dz$$
(11)

In the end, the variation of works done by external forces can be computed as:

$$\delta V = \int_{-\frac{h}{2}}^{\frac{h}{2}} \int_0^{2\pi} \int_0^L \left(N_r + N_x\frac{\partial^2 w}{\partial x^2} + \frac{N_\phi}{R^2}\frac{\partial^2 w}{\partial \phi^2} + k_w + k_p\left(\frac{\partial^2 w}{\partial x^2} + \frac{1}{R^2}\frac{\partial^2 w}{\partial \phi^2}\right)\right)\delta w R dx d\phi dz$$
(12)

Three types of loadings act on the cylindrical shell by names of radial loading (N_r), axial loading (N_x), and circumferential loading (N_ϕ). Additionally, there are two coefficients, K_w, and K_p, which represent the Winkler and Pasternak properties of the elastic substrate, respectively. To study the buckling behavior, the applied buckling load (N_b) replaces the axial loading of in the equations. Once equations (11) and (12) are inserted into equation (10), the motion equations for the cylindrical shell can be determined by considering elastic properties. These motion equations can be shown as [26]:

$$\frac{\partial N_{xx}}{\partial x} + \frac{1}{R}\frac{\partial N_{x\phi}}{\partial \phi} = 0 \tag{13}$$

$$\frac{\partial N_{x\phi}}{\partial x} + \frac{1}{R}\frac{\partial N_{\phi\phi}}{\partial \phi} + \frac{Q_{z\phi}}{R} + N^b\frac{\partial^2 v}{\partial x^2} = 0 \tag{14}$$

$$\frac{\partial Q_{xz}}{\partial x} + \frac{1}{R}\frac{\partial Q_{z\phi}}{\partial \phi} - \frac{N_{\phi\phi}}{R} - k_w + k_p\left(\frac{\partial^2 w}{\partial x^2} + \frac{1}{R^2}\frac{\partial^2 w}{\partial \phi^2}\right) + N^b\frac{\partial^2 w}{\partial x^2} = 0, \tag{15}$$

$$\frac{\partial M_{xx}}{\partial x} + \frac{1}{R}\frac{\partial M_{x\phi}}{\partial \phi} - Q_{xz} = 0, \tag{16}$$

$$\frac{\partial M_{x\phi}}{\partial x} + \frac{1}{R}\frac{\partial M_{\phi\phi}}{\partial \phi} - Q_{\phi z} = 0, \tag{17}$$

Where:

$$\begin{aligned}
[N_{xx}, N_{\phi\phi}, N_{x\phi}] &= \int_{-\frac{h}{2}}^{\frac{h}{2}}[\sigma_{xx}, \sigma_{\phi\phi}, \sigma_{x\phi}]\,\mathrm{dz}, \\
[M_{xx}, M_{\phi\phi}, M_{x\phi}] &= \int_{-\frac{h}{2}}^{\frac{h}{2}}[\sigma_{xx}, \sigma_{\phi\phi}, \sigma_{x\phi}]\,z\mathrm{dz}, \\
[Q_{xz}, Q_{\phi z}] &= \kappa_S\int_{-\frac{h}{2}}^{\frac{h}{2}}[\sigma_{xz}, \sigma_{z\phi}]\,\mathrm{dz}
\end{aligned} \tag{18}$$

In which κ_S is the shear correction factor.

2.4. Constitutive equations

The following equation shows the relation between stress and strain in a nanocomposite as:

$$(\sigma_{ij} = C_{ijkl}\varepsilon_{kl}) \tag{19}$$

considering three important properties: stress, strain, and elasticity that are used in the formation of the Cauchy stress tensor (σ_{ij}), the strain tensor (ε_{kl}), and the elasticity tensor (C_{ijkl}) in these equations. By integrating the equation provided over the thickness of the shell a relation between these tensors is obtained. The following relations are used to define the behavior [26]:

$$\begin{bmatrix} N_{xx} \\ M_{xx} \\ N_{\phi\phi} \\ M_{\phi\phi} \end{bmatrix} = \begin{bmatrix} A_{11} & B_{11} & \dfrac{A_{12}}{R} & \dfrac{B_{12}}{R} \\ B_{11} & D_{11} & \dfrac{B_{12}}{R} & \dfrac{D_{12}}{R} \\ A_{12} & B_{12} & \dfrac{A_{11}}{R} & \dfrac{B_{11}}{R} \\ B_{12} & D_{12} & \dfrac{B_{11}}{R} & \dfrac{D_{11}}{R} \end{bmatrix} \begin{bmatrix} \dfrac{\partial u}{\partial x} \\ \dfrac{\partial \theta_x}{\partial x} \\ \dfrac{\partial v}{\partial \phi} + w \\ \dfrac{\partial \theta_\phi}{\partial \phi} \end{bmatrix},$$

$$\begin{bmatrix} N_{x\phi} \\ M_{x\phi} \end{bmatrix} = \begin{bmatrix} A_{66} & B_{66} \\ B_{66} & D_{66} \end{bmatrix} \begin{bmatrix} \dfrac{1}{R}\dfrac{\partial u}{\partial \phi} + \dfrac{\partial v}{\partial x} \\ \dfrac{1}{R}\dfrac{\partial \theta_x}{\partial \phi} + \dfrac{\partial \theta_\phi}{\partial x} \end{bmatrix}$$

$$Q_{xz} = A_{55}^{S}\left(\theta_x + \frac{\partial w}{\partial x}\right), Q_{\phi z} = A_{55}^{S}\left(\theta_\phi + \frac{1}{R}\frac{\partial w}{\partial \phi} - \frac{v}{R}\right)$$

(20)

Where:

$$[A_{11}, B_{11}, D_{11}] = \int_{-\frac{h}{2}}^{\frac{h}{2}} [1, z, z^2] \frac{E_{11}}{1 - v_{12}v_{21}}\, dz$$

$$[A_{12}, B_{12}, D_{12}] = \int_{-\frac{h}{2}}^{\frac{h}{2}} [1, z, z^2] \frac{v_{12}E_{22}}{1 - v_{12}v_{21}}\, dz$$

$$[A_{66}, B_{66}, D_{66}] = \int_{-\frac{h}{2}}^{\frac{h}{2}} [1, z, z^2] \frac{E_{11}}{2(1 + v_{12})}\, dz$$

$$A_{55}^{S} = \kappa_S \int_{-\frac{h}{2}}^{\frac{h}{2}} \frac{E_{11}}{2(1 + v_{12})}\, dz$$

(21)

2.5. Governing equations

Subsequently, the governing partial differential equations of NC shell under study can be formulated in the following form as:

$$A_{11}\frac{\partial^2 u}{\partial x^2} + B_{11}\frac{\partial^2 \theta_x}{\partial x^2} + \frac{A_{12}}{R}\left(\frac{\partial^2 v}{\partial x \partial \phi} + \frac{\partial w}{\partial x}\right) + \frac{B_{12}}{R}\frac{\partial^2 \theta_\phi}{\partial x \partial \phi} + \frac{A_{66}}{R}\left(\frac{1}{R}\frac{\partial^2 u}{\partial \phi^2}\right.$$
$$\left. + \frac{\partial^2 v}{\partial x \partial \phi}\right) + \frac{B_{66}}{R}\left(\frac{1}{R}\frac{\partial^2 \theta_x}{\partial \phi^2} + \frac{\partial^2 \theta_\phi}{\partial x \partial \phi}\right) = 0$$

(22)

$$\left(A_{66}\left(\frac{1}{R}\frac{\partial^2 u}{\partial x \partial \phi} + \frac{\partial^2 v}{\partial x^2}\right) + B_{66}\left(\frac{1}{R}\frac{\partial^2 \theta_x}{\partial x \partial \phi} + \frac{\partial^2 \theta_\phi}{\partial x^2}\right) + \frac{A_{12}}{R}\frac{\partial^2 u}{\partial x \partial \phi}\right)(+\frac{B_{12}}{R}\frac{\partial^2 \theta_x}{\partial x \partial \phi} + \frac{A_{11}}{R^2}\left(\frac{\partial^2 v}{\partial \phi^2} + \frac{\partial w}{\partial \phi}\right)$$
$$+ \frac{B_{11}}{R^2}\frac{\partial^2 \theta_\phi}{\partial \phi^2} +)(\frac{A_{55}^{S}}{R}\left(\theta_\phi + \frac{1}{R}\frac{\partial w}{\partial \phi} - \frac{v}{R}\right) + N^b\frac{\partial^2 v}{\partial x^2} = 0),$$

(23)

$$A_{55}^{S}\left(\frac{\partial \theta_x}{\partial x} + \frac{\partial^2 w}{\partial x^2}\right) + \frac{A_{55}^{S}}{R}\left(\frac{\partial \theta_\phi}{\partial \phi} + \frac{1}{R}\frac{\partial^2 w}{\partial \phi^2} - \frac{1}{R}\frac{\partial v}{\partial \phi}\right) - \frac{A_{12}}{R}\frac{\partial u}{\partial x}$$
$$- \frac{B_{12}}{R}\frac{\partial \theta_x}{\partial x} - \frac{A_{11}}{R^2}\left(\frac{\partial v}{\partial \phi} + w\right) - k_w +$$
$$k_p\left(\frac{\partial^2 w}{\partial x^2} + \frac{1}{R^2}\frac{\partial^2 w}{\partial \phi^2}\right) + N^b\frac{\partial^2 w}{\partial x^2} = 0,$$

(24)

$$B_{11}\frac{\partial^2 u}{\partial x^2} + D_{11}\frac{\partial^2 \theta_x}{\partial x^2} + \frac{B_{12}}{R}\left(\frac{\partial^2 v}{\partial x \partial \phi} + \frac{\partial w}{\partial x}\right) + \frac{D_{12}}{R}\frac{\partial^2 \theta_\phi}{\partial x \partial \phi} + \frac{B_{66}}{R}\left(\frac{1}{R}\frac{\partial^2 u}{\partial \phi^2}\right)$$

$$+ \frac{\partial^2 v}{\partial x \partial \phi}\right) + \frac{D_{66}}{R}\left(\frac{1}{R}\frac{\partial^2 \theta_x}{\partial \phi^2} + \frac{\partial^2 \theta_\phi}{\partial x \partial \phi}\right) - A_{55}^s\left(\theta_x + \frac{\partial w}{\partial x}\right) = 0, \tag{25}$$

$$B_{66}\left(\frac{1}{R}\frac{\partial^2 u}{\partial x \partial \phi} + \frac{\partial^2 v}{\partial x^2}\right) + D_{66}\left(\frac{1}{R}\frac{\partial^2 \theta_x}{\partial x \partial \phi} + \frac{\partial^2 \theta_\phi}{\partial x^2}\right) + \frac{B_{12}}{R}\frac{\partial^2 u}{\partial x \partial \phi}$$

$$+ \frac{D_{12}}{R}\frac{\partial^2 \theta_x}{\partial x \partial \phi} + \frac{B_{11}}{R^2}\left(\frac{\partial^2 v}{\partial \phi^2} + \frac{\partial w}{\partial \phi}\right) + \frac{D_{11}}{R^2}\frac{\partial^2 \theta_\phi}{\partial \phi^2} - \tag{26}$$

$$A_{55}^s\left(\theta_\phi + \frac{1}{R}\frac{\partial w}{\partial \phi} - \frac{v}{R}\right) = 0$$

2.6. Solution method

In this section, Galerkin's method is utilized to find out the shell's buckling behavior. This method is used to determine the critical buckling load. According to this methodology, the displacement field is obtained from the following set of equations:

$$u = \sum_{m=1}^{\infty}\sum_{n=1}^{\infty} U_{mn}\frac{\partial X_m(x)}{\partial x}\cos(n\phi),$$

$$v = \sum_{m=1}^{\infty}\sum_{n=1}^{\infty} V_{mn}X_m(x)\sin(n\phi),$$

$$w = \sum_{m=1}^{\infty}\sum_{n=1}^{\infty} W_{mn}X_m(x)\cos(n\phi), \tag{27}$$

$$\theta_x = \sum_{m=1}^{\infty}\sum_{n=1}^{\infty} \Theta_{xmn}\frac{\partial X_m(x)}{\partial x}\cos(n\phi),$$

$$\theta_\phi = \sum_{m=1}^{\infty}\sum_{n=1}^{\infty} \Theta_{\phi mn}X_m(x)\sin(n\phi)$$

Unknown coefficients are represented by U_{mn}, V_{mn}, W_{mn}, Θ_{xmn}, and $\Theta_{\phi mn}$. Additionally, n denotes the circumferential wave numbers and X_m is a function used to satisfy the axial boundary conditions. For a S-S boundary condition we have:

$$w = \frac{\partial^2 w}{\partial x^2} = 0 \text{ at } x = 0, L \tag{28}$$

Now, the buckling load of the shell can be determined by inserting equations (22) – (26) into equation (27), and by doing so, the factor that led the shell to buckle or collapse is revealed which is the critical load. For identifying the critical buckling load values, the following eigenvalue problem must be solved:

$$[K]\Delta = 0 \tag{29}$$

Where Δ denotes the column vector containing the unknown coefficients, also, the stiffness matrix is represented by K. The X_m function satisfying the S-S boundary condition is assumed to be as follows:

$$S - S: \quad X_m = sin(\frac{m\pi x}{L}) \tag{30}$$

3. Numerical results

The focus of this part is on presenting numerical results to understand how different factors affect the buckling behavior of a nanocomposite shell reinforced with GPL fibers. The shell is primarily made of epoxy material and it is reinforced with GPLs. The material properties of both the epoxy and GPL fibers are taken from reference papers [24, 46]. The thickness of the shell is assumed to be 5cm (*h=5cm*). Various illustrations are presented to study the impact of different parameters on the stability of the nanocomposite shell. The accuracy of the methodology used in this study has been validated by comparing the results with those from previous research that focused on the buckling analysis of shells (Table 1).

Table 1. Comparison of the critical buckling load of cylindrical shells.

		Source and method	
R/t	*L/R*	Wang et al.[47] via FEM	Present work via analytical method
30	2	499,602	498,539
	3	489,986	488,740
	4	485,494	486,322
40	2	498,381	499,212
	3	488,982	490,004
	4	485,396	481,673
50	2	496,553	482,956
	3	488,608	479,188
	4	485,805	474,012

The discrepancies in results is due to the fact that the previous study conducted by Wang et al. [47] used finite element analysis, while this paper uses an analytical method to extract the buckling loads. Naturally, it is expected to encounter some discrepancies when setting both results side by side. Nevertheless, the agreement between the results from this work and those from other studies in the literature confirms the reliability and accuracy of the presented methodology. Herein, the subsequent dimensionless parameters are established to enhance simplicity.

$$N_{cr} = \frac{N^b}{100 E_m h^2 / R \sqrt{3(1-v_m)}}, \quad K_w = \frac{k_w L^4}{E_m h^3 / 12(1-v_m^2)}, \quad K_p = \frac{k_p L^2}{E_m h^3 / 12(1-v_m^2)} \tag{31}$$

In the figures delineated below how various parameters such as weight fractions of GPLs, foundation properties, circumferential wave number, and shell geometry influence the buckling behavior of GPL-reinforcement (GPLR) nanocomposite shells is studied. These factors affect the stiffness and stability of the nanocomposite shells, leading to variations in the critical buckling loads. So, in detail: In Figures 2 to 6, the effects of different factors on the buckling behavior of GPLR nanocomposite shells are demonstrated.
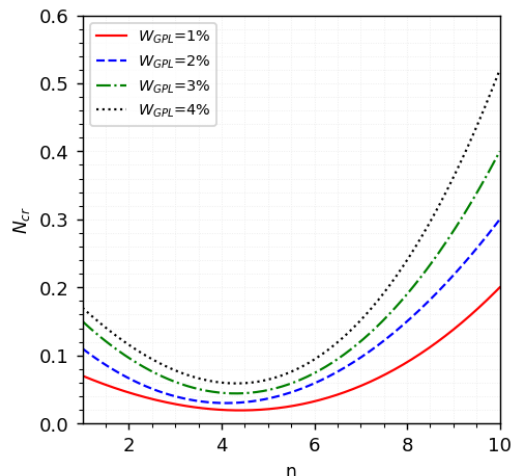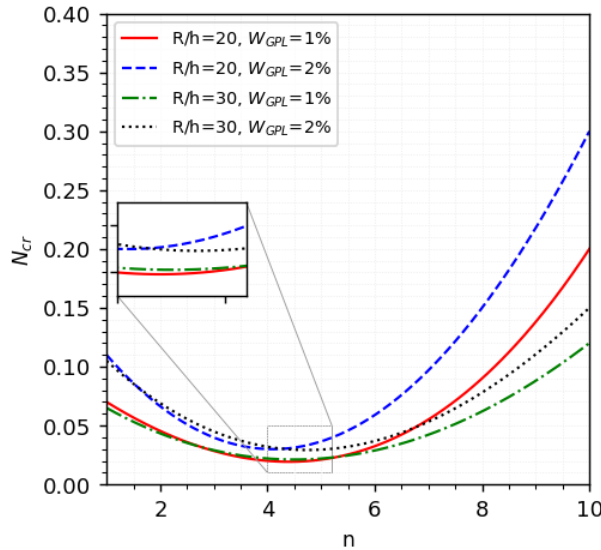

Figure 2. Variation of the dimensionless buckling load of S-S nanocomposite shells against circumferential wave number (n) for various weight fractions of GOPs (*L/h=R/h=20*).

Figure 2 shows how changing the weight fraction of GPLs influences the buckling loads of GPLR shells, considering a constant ratio of *L/h* and *R/h* at *L/h = R/h = 20*. It is evident that GPLR shells with lower weight fractions has lower critical buckling loads compared to those with higher weight fractions. So, increasing the weight fraction of GPLs enhances the buckling loads of GPLR shells. This means that higher stability can be achieved by adding more weight fraction of GPLs.
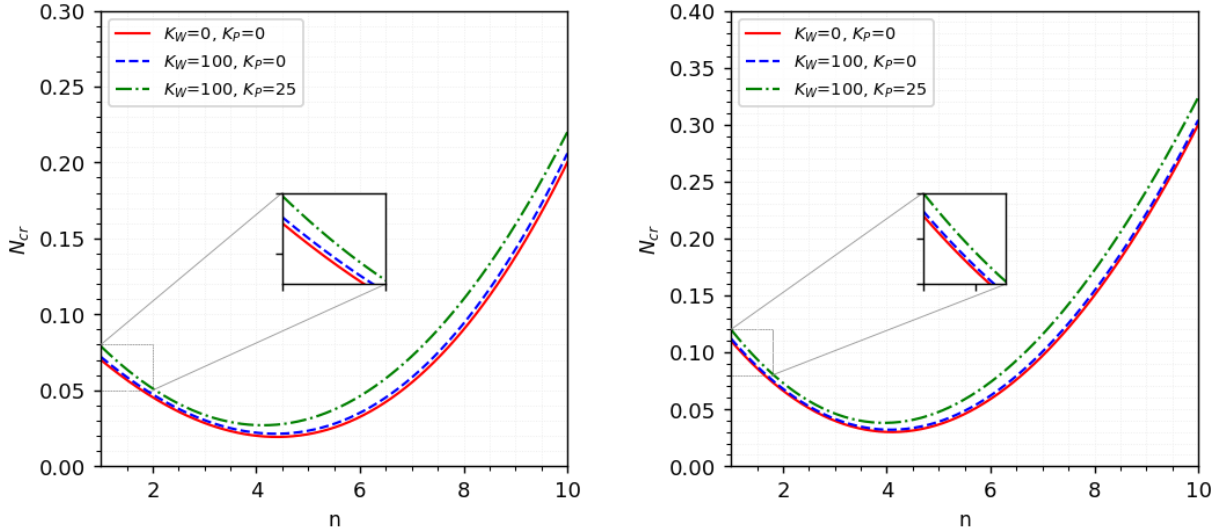
Figure 3. Variation of the dimensionless buckling load of S-S nanocomposite shells versus circumferential wave number (n) for various foundation parameters at (a) *W$_{GPL}$=1%*, and (b) *W$_{GPL}$=2%* (*L/h=R/h=20*).

Figure 3 highlights the effects of Winkler (K_w) and Pasternak (K_p) foundation parameters on the buckling loads of GPLR nanocomposite shells, with different weight fractions of GPLs. The presence of an elastic medium significantly affects the buckling behavior of GPLR structure, making the structure stiffer, thus increasing the buckling load. Moreover, the buckling load also depend on the value of the circumferential wave number. Increasing the circumferential wave number initially reduces the dimensionless buckling loads, but then they start to increase continuously with each magnitude of Winkler and Pasternak coefficients, irrespective of the weight fraction.

Figure 4. Variation of the dimensionless buckling load of S-S nanocomposite shells versus circumferential wave number (n) for different radius-to-thickness ratios and weight fractions of GPLs (*L/h=20*).

Moreover, in Figures 4 and 5, the effects of different radius-to-thickness and length-to-thickness ratios, respectively, are demonstrated. Lower values of circumferential wave numbers show no significant difference in the buckling behavior of the nanocomposite shells. However, at higher circumferential wave numbers, lower radius-to-

thickness ratio and higher length-to-thickness ratio, with constant *L/h* and *R/h* ratios, respectively, increase the stiffness of the nanocomposite and lead to higher buckling loads. As shown in Figure 2, higher weight fractions also lead to higher buckling loads at constant values of either length-to-thickness or radius-to-thickness ratios.
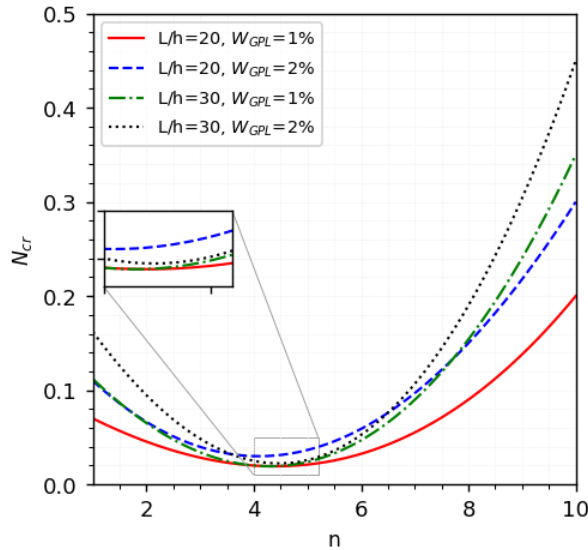
Figure 5. Variation of the dimensionless buckling load of S-S nanocomposite shells versus circumferential wave number (n) for different length-to-thickness ratios and weight fractions of GPLs (*R/h=20*).

Figure 6 emphasizes the influences of elastic foundation coefficients on the dimensionless buckling loads of GPLR nanocomposite shells. The critical buckling load increases linearly with the increase in Winkler and Pasternak parameters, as it enhances the stiffness of the GPLR nanocomposite. Additionally, it is evident that the Pasternak foundation has a more significant effect in increasing buckling loads compared to the Winkler foundation. Furthermore, it is clear that the Pasternak foundation has a stronger influence on the rise of buckling loads than the Winkler foundation.

$K_P = 10$ $K_W = 50$
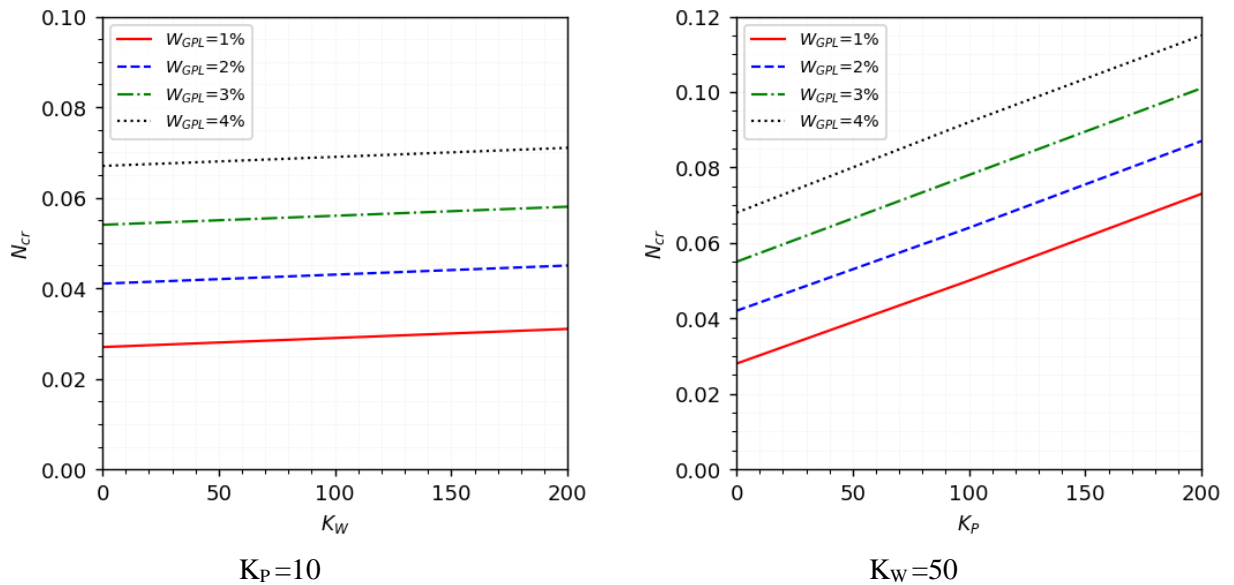
Figure 6. Variation of the dimensionless buckling load of S-S nanocomposite shells versus foundation coefficients for various weight fractions of GOPs whenever (a) variable Winkler coefficient, and (b) variable Pasternak coefficient (*L/h=R/h=20*).

4. Conclusion

In this manuscript, the buckling characteristics of graphene platelets reinforced (GPLR) nanocomposite shells were scrutinized utilizing the first-order shear deformation theory. To amalgamate the material properties, Halpin-Tsai equations were employed. Solutions to the governing differential equations were attained through the rigorous application of Galerkin's method. These analytical solutions showcased strong concordance with established results from prior analyses. Inference from the calculations indicates a marked augmentation in the critical buckling load of the GPLR nanocomposite shells correlating with increases in GPLs' weight fraction, regardless of other influencing factors. Further observations revealed an upturn in critical buckling loads with higher values of circumferential wave numbers, concurrently with diminished radius-to-thickness and augmented length-to-thickness ratios, at consistent sectional ratios of *L/h* and *R/h*. Additionally, the study revealed that both Winkler and Pasternak foundation parameters play a pivotal role in elevating the critical buckling loads, with the influence of the Pasternak parameter being substantially more pronounced compared to that of the Winkler parameter. In the context of graphene platelets, as previously discussed in the research, its distinctive strength is anticipated to lead to increased adoption during the projected timeframe. These attributes have the potential to fuel demand for graphene platelets in the coming years.

References

[1]   C. Lee, X. Wei, J. W. Kysar, J. Hone, Measurement of the elastic properties and intrinsic strength of monolayer graphene, *science,* Vol. 321, No. 5887, pp. 385-388, 2008.

[2]   M. Rafiee, J. Rafiee, Z.-Z. Yu, N. Koratkar, Buckling resistant graphene nanocomposites, *Applied Physics Letters,* Vol. 95, No. 22, 2009.

[3]   G. Formica, W. Lacarbonara, R. Alessi, Vibrations of carbon nanotube-reinforced composites, *Journal of sound and vibration,* Vol. 329, No. 10, pp. 1875-1889, 2010.

[4]   R. Kolahchi, M. Safari, M. Esmailpour, Dynamic stability analysis of temperature-dependent functionally graded CNT-reinforced visco-plates resting on orthotropic elastomeric medium, *Composite Structures,* Vol. 150, pp. 255-265, 2016.

[5]   M. Nejati, R. Dimitri, F. Tornabene, M. Hossein Yas, Thermal buckling of nanocomposite stiffened cylindrical shells reinforced by functionally graded wavy carbon nanotubes with temperature-dependent properties, *Applied Sciences,* Vol. 7, No. 12, pp. 1223, 2017.

[6]   M. R. Barati, A. M. Zenkour, Post-buckling analysis of refined shear deformable graphene platelet reinforced beams with porosities and geometrical imperfection, *Composite Structures,* Vol. 181, pp. 194-202, 2017.

[7]   J. Yang, H. Wu, S. Kitipornchai, Buckling and postbuckling of functionally graded multilayer graphene platelet-reinforced composite beams, *Composite Structures,* Vol. 161, pp. 111-118, 2017.

[8]   Y. Wang, C. Feng, Z. Zhao, F. Lu, J. Yang, Torsional buckling of graphene platelets (GPLs) reinforced functionally graded cylindrical shell with cutout, *Composite Structures,* Vol. 197, pp. 72-79, 2018.

[9]   H. Golabchi, R. Kolahchi, M. R. Bidgoli, Vibration and instability analysis of pipes reinforced by SiO2 nanoparticles considering agglomeration effects, *Computers and Concrete, An International Journal,* Vol. 21, No. 4, pp. 431-440, 2018.

[10]   J. Yang, D. Chen, S. Kitipornchai, Buckling and free vibration analyses of functionally graded graphene reinforced porous nanocomposite plates based on Chebyshev-Ritz method, *Composite Structures,* Vol. 193, pp. 281-294, 2018.

[11]   M. H. Hajmohammad, M. Maleki, R. Kolahchi, Seismic response of underwater concrete pipes conveying fluid covered with nano-fiber reinforced polymer layer, *Soil Dynamics and Earthquake Engineering,* Vol. 110, pp. 18-27, 2018.

[12]   X. Chen, Z. Qiu, Reliability assessment of fiber-reinforced composite laminates with correlated elastic mechanical parameters, *Composite Structures,* Vol. 203, pp. 396-403, 2018.

[13]   M. H. Hajmohammad, A. H. Nouri, M. S. Zarei, R. Kolahchi, A new numerical approach and visco-refined zigzag theory for blast analysis of auxetic honeycomb plates integrated by multiphase nanocomposite facesheets in hygrothermal environment, *Engineering with Computers,* Vol. 35, pp. 1141-1157, 2019.

[14]   Y. Wang, C. Feng, C. Santiuste, Z. Zhao, J. Yang, Buckling and postbuckling of dielectric composite beam reinforced with Graphene Platelets (GPLs), *Aerospace Science and Technology,* Vol. 91, pp. 208-218, 2019.

[15] Z. Zhou, Y. Ni, Z. Tong, S. Zhu, J. Sun, X. Xu, Accurate nonlinear buckling analysis of functionally graded porous graphene platelet reinforced composite cylindrical shells, *International Journal of Mechanical Sciences,* Vol. 151, pp. 537-550, 2019.

[16] F. Ebrahimi, Buckling analysis of graphene oxide powder-reinforced nanocomposite beams subjected to non-uniform magnetic field, *Structural Engineering and Mechanics, An Int'l Journal,* Vol. 71, No. 4, pp. 351-361, 2019.

[17] Z. Qin, B. Safaei, X. Pang, F. Chu, Traveling wave analysis of rotating functionally graded graphene platelet reinforced nanocomposite cylindrical shells with general boundary conditions, *Results in Physics,* Vol. 15, pp. 102752, 2019.

[18] R. B. Mahani, A. Eyvazian, F. Musharavati, T. A. Sebaey, P. Talebizadehsardari, Thermal buckling of laminated Nano-Composite conical shell reinforced with graphene platelets, *Thin-Walled Structures,* Vol. 155, pp. 106913, 2020.

[19] B. Keshtegar, A. Farrokhian, R. Kolahchi, N.-T. Trung, Dynamic stability response of truncated nanocomposite conical shell with magnetostrictive face sheets utilizing higher order theory of sandwich panels, *European Journal of Mechanics-A/Solids,* Vol. 82, pp. 104010, 2020.

[20] M.-H. Yas, S. Rahimi, Thermal buckling analysis of porous functionally graded nanocomposite beams reinforced by graphene platelets using Generalized differential quadrature method, *Aerospace Science and Technology,* Vol. 107, pp. 106261, 2020.

[21] B. Keshtegar, M. Motezaker, R. Kolahchi, N.-T. Trung, Wave propagation and vibration responses in porous smart nanocomposite sandwich beam resting on Kerr foundation considering structural damping, *Thin-Walled Structures,* Vol. 154, pp. 106820, 2020.

[22] R. Kolahchi, S.-P. Zhu, B. Keshtegar, N.-T. Trung, Dynamic buckling optimization of laminated aircraft conical shells with hybrid nanocomposite martial, *Aerospace Science and Technology,* Vol. 98, pp. 105656, 2020.

[23] M. Song, Y. Gong, J. Yang, W. Zhu, S. Kitipornchai, Nonlinear free vibration of cracked functionally graded graphene platelet-reinforced nanocomposite beams in thermal environments, *Journal of Sound and Vibration,* Vol. 468, pp. 115115, 2020.

[24] Z. Zhang, Y. Li, H. Wu, H. Zhang, H. Wu, S. Jiang, G. Chai, Mechanical analysis of functionally graded graphene oxide-reinforced composite beams based on the first-order shear deformation theory, *Mechanics of Advanced Materials and Structures,* Vol. 27, No. 1, pp. 3-11, 2020.

[25] F. Abbaspour, H. Arvin, Thermo-electro-mechanical buckling analysis of sandwich nanocomposite microplates reinforced with graphene platelets integrated with piezoelectric facesheets resting on elastic foundation, *Computers & Mathematics with Applications,* Vol. 101, pp. 38-50, 2021.

[26] F. Ebrahimi, P. Hafezi, A. Dabbagh, Buckling analysis of embedded graphene oxide powder-reinforced nanocomposite shells, *Defence Technology,* Vol. 17, No. 1, pp. 226-233, 2021.

[27] D. Shahgholian-Ghahfarokhi, G. Rahimi, A. Khodadadi, H. Salehipour, M. Afrand, Buckling analyses of FG porous nanocomposite cylindrical shells with graphene platelet reinforcement subjected to uniform external lateral pressure, *Mechanics Based Design of Structures and Machines,* Vol. 49, No. 7, pp. 1059-1079, 2021.

[28] D. Shahgholian-Ghahfarokhi, M. Safarpour, A. Rahimi, Torsional buckling analyses of functionally graded porous nanocomposite cylindrical shells reinforced with graphene platelets (GPLs), *Mechanics Based Design of Structures and Machines,* Vol. 49, No. 1, pp. 81-102, 2021.

[29] M. Al-Furjan, A. Farrokhian, B. Keshtegar, R. Kolahchi, N.-T. Trung, Dynamic stability control of viscoelastic nanocomposite piezoelectric sandwich beams resting on Kerr foundation based on exponential piezoelasticity theory, *European Journal of Mechanics-A/Solids,* Vol. 86, pp. 104169, 2021.

[30] R. Ansari, R. Hassani, R. Gholami, H. Rouhi, Free vibration analysis of postbuckled arbitrary-shaped FG-GPL-reinforced porous nanocomposite plates, *Thin-Walled Structures,* Vol. 163, pp. 107701, 2021.

[31] M. Al-Furjan, A. Farrokhian, S. Mahmoud, R. Kolahchi, Dynamic deflection and contact force histories of graphene platelets reinforced conical shell integrated with magnetostrictive layers subjected to low-velocity impact, *Thin-Walled Structures,* Vol. 163, pp. 107706, 2021.

[32] R. Kolahchi, F. Kolahdouzan, A numerical method for magneto-hygro-thermal dynamic stability analysis of defective quadrilateral graphene sheets using higher order nonlocal strain gradient theory with different movable boundary conditions, *Applied Mathematical Modelling,* Vol. 91, pp. 458-475, 2021.

[33] J. Zheng, C. Zhang, F. Musharavati, A. Khan, T. A. Sebaey, A. Eyvazian, Forced vibration characteristics of embedded graphene oxide powder reinforced metal foam nanocomposite plate in thermal environment, *Case Studies in Thermal Engineering,* Vol. 27, pp. 101167, 2021.

[34] E. Sobhani, M. Avcar, The influence of various nanofiller materials (CNTs, GNPs, and GOPs) on the natural frequencies of nanocomposite cylindrical shells: a comparative study, *Materials Today Communications,* Vol. 33, pp. 104547, 2022.

[35] F. Ebrahimi, M. Nouraei, A. Seyfi, Wave dispersion characteristics of thermally excited graphene oxide powder-reinforced nanocomposite plates, *Waves in Random and Complex Media,* Vol. 32, No. 1, pp. 204-232, 2022.

[36] E. Sobhani, A. R. Masoodi, O. Civalek, A. R. Ahmadi-Pari, Agglomerated impact of CNT vs. GNP nanofillers on hybridization of polymer matrix for vibration of coupled hemispherical-conical-conical shells, *Aerospace Science and Technology,* Vol. 120, pp. 107257, 2022.

[37] M. Guo, H. Arvin, Nonlinear thermal buckling instability analysis of a rotating nanocomposite beam reinforced with graphene platelet via the Chebyshev–Ritz scheme, *Engineering Analysis with Boundary Elements,* Vol. 146, pp. 241-251, 2023.

[38] Z. Li, Q. Zhang, H. Shen, X. Xiao, H. Kuai, J. Zheng, Buckling performance of the encased functionally graded porous composite liner with polyhedral shapes reinforced by graphene platelets under external pressure, *Thin-Walled Structures,* Vol. 183, pp. 110370, 2023.

[39] O. Ahmadi, S. Rash-Ahmadi, Geometrically nonlinear post-buckling of advanced porous nanocomposite lying on elastic foundation in hygrothermal environment, *Acta Mechanica*, pp. 1-19, 2023.

[40] J. Xiang, Y. Lai, Z. Moradi, M. Khorami, Wave propagation phenomenon of functionally graded graphene oxide powder-strengthened nanocomposite curved beam, *Solid State Communications,* Vol. 369, pp. 115193, 2023.

[41] F. Ebrahimi, H. Ezzati, M. Najafi, Wave propagation analysis of functionally graded nanocomposite plate reinforced with graphene platelets in presence of thermal excitation, *Acta Mechanica*, pp. 1-20, 2023.

[42] S. Bi, E. Zhang, M. Babaei, F. Tornabene, R. Dimitri, The Influence of GPL Reinforcements on the Post-Buckling Behavior of FG Porous Rings Subjected to an External Pressure, *Mathematics,* Vol. 11, No. 11, pp. 2421, 2023.

[43] F. Ebrahimi, M. Nouraei, A. Dabbagh, Thermal vibration analysis of embedded graphene oxide powder-reinforced nanocomposite plates, *Engineering with Computers,* Vol. 36, pp. 879-895, 2020.

[44] S. Qaderi, F. Ebrahimi, Vibration analysis of polymer composite plates reinforced with graphene platelets resting on two-parameter viscoelastic foundation, *Engineering with Computers*, pp. 1-17, 2022.

[45] N. Vu-Bac, T. Duong, T. Lahmer, P. Areias, R. Sauer, H. Park, T. Rabczuk, A NURBS-based inverse analysis of thermal expansion induced morphing of thin shells, *Computer Methods in Applied Mechanics and Engineering,* Vol. 350, pp. 480-510, 2019.

[46] J. Liu, H. Yan, K. Jiang, Mechanical properties of graphene platelet-reinforced alumina ceramic composites, *Ceramics International,* Vol. 39, No. 6, pp. 6215-6221, 2013.

[47] Y. Wang, C. Feng, Z. Zhao, J. Yang, Eigenvalue buckling of functionally graded cylindrical shells reinforced with graphene platelets (GPL), *Composite Structures,* Vol. 202, pp. 38-46, 2018.